Astronomy & Astrophysics manuscript no. output
March 23, 2026

Hayabusa2# enstatite-like target 1998 KY_{26} originating from the Nysa family

Eri Tatsumi[1,2,3], Julia de León[1,2], and Marcel M. Popescu[4,5]

[1] Instituto de Astrofísica de Canarias (IAC), C/Vía Láctea s/n, 38205 La Laguna, Tenerife, Spain
e-mail: eri.tatsumi@iac.es
[2] Departamento de Astrofísica, Universidad de La Laguna, Avda. Astrofísico Francisco Sánchez, 38206 La Laguna, Tenerife, Spain
[3] University of Tokyo, Bunkyo-ku, 133-0033, Tokyo, Japan
[4] Institute of Space Science – INFLPR Subsidiary, 409 Atomiştilor Street, Măgurele, Ilfov, 077125, Romania
[5] University of Craiova, Alexandru Ioan Cuza 13, Craiova, 200585, Romania

Received xxx, 2025

ABSTRACT

Context. Following its nominal mission, the Hayabusa2 spacecraft is cruising toward two new targets as part of its extended mission, Hayabusa2# (SHARP: Small Hazardous Asteroid Reconnaissance Probe). The spacecraft will fly by the near-Earth asteroid (98943) Torifune in 2026 and rendezvous with another near-Earth asteroid, 1998 KY_{26}, in 2031. 1998 KY_{26} was at its brightest in 2024 since its discovery in 1998.
Aims. This study aims to characterize the surface composition of 1998 KY_{26} and constrain its origin.
Methods. We used the 10.4-meter Gran Telescopio Canarias to obtain a visible reflectance spectrum of 1998 KY_{26} in May 2024. We analyzed the spectrum for taxonomic classification and compared it with laboratory meteoritic spectra and other E-type asteroids.
Results. The spectrum of 1998 KY_{26} shows an overall positive spectral slope with no clear absorption feature, which turns flat (neutral) at 0.6-0.7 μm and slightly negative toward 0.9 μm. It is taxonomically classified as an Xe-type (Bus-DeMeo) or X-type (Tholen), while the asteroid's high geometric albedo ($p_V \sim 0.52$) identifies 1998 KY26 as an E-type (Tholen). The spectral shape is consistent with enstatite chondrites (EL/EH).
Conclusions. Considering the spectral shape and the high albedo of 1998 KY_{26}, it quite likely originated from the inner main belt rather than the Hungaria region. These results also suggest a possible relationship to asteroids (44) Nysa and (135) Hertha, which may originate from layers of different reduction states in a parent body.

Key words. Minor planets, asteroids: individual: 1998 KY_{26}— Hayabusa2# — Techniques: spectroscopic

1. Introduction

Following its successful sample return from the carbonaceous asteroid (162173) Ryugu, the Japanese Aerospace Exploration Agency's (JAXA) Hayabusa2 spacecraft transitioned to the ambitious extended mission, Hayabusa2# (SHARP: Small Hazardous Asteroid Reconnaissance Probe). This new phase of its journey will see Hayabusa2 undertake a long cruise, including a close flyby of the near-Earth asteroid (98943) Torifune in 2026, before ultimately reaching its primary target, the near-Earth asteroid 1998 KY_{26}, in 2031 (Hirabayashi et al. 2021).

Asteroid 1998 KY_{26} is a particularly intriguing object for scientific study due to its tiny size and exceptionally fast rotation. With an estimated diameter of only about 30 meters, the asteroid's rapid spin period of approximately 10 minutes per rotation, as observed at the time of its discovery (Ostro et al. 1999), makes it truly unique. Recently, several studies have suggested an even faster rotation up to $\sim$ 5 min for this object, leading to an even smaller diameter of less than 15 meters (Beniyama et al. 2025; Santana-Ros et al. 2025). This small rapid rotator poses both significant challenges for close-up observations and presents unparalleled opportunities to investigate the physical properties and internal structures of such fast-spinning, small celestial bodies (e.g., Kikuchi et al. 2023).

The study of small (meter - to tens-of-meter-sized) near-Earth asteroids such as 1998 KY_{26} has gained considerable importance in recent years, particularly within the burgeoning field of planetary defense, which encompasses global efforts to identify, track, and mitigate the potential threat of asteroid impacts on Earth. A good example is the impact, which occurred on February 15, 2013, when a 17-20 m diameter asteroid entered the atmosphere over Chelyabinsk, Russia, and exploded in an airburst that liberated about 500 kilotons of TNT equivalent (Brown et al. 2013). Other examples are the recent cases of the 30 m E-type asteroid 2023 DZ_2 (Popescu et al. 2023; Reddy et al. 2024) – which has a minimum orbit intersection distance (MOID) with Earth of 0.00005 au as well as an unusually high initial probability of near-term impact – and the 60 meter asteroid 2024 YR_4 (Rivkin et al. 2025), which reached an impact probability of $\sim$3% early in 2025. Understanding the characteristics and behaviors of these small asteroids, which are more numerous and often hard to detect, is crucial for developing effective strategies to protect our planet from future collisions.

2. Spectroscopic observations and data reduction

Despite its discovery in 1998, favorable observing windows for 1998 KY_{26} are infrequent. April and May 2024 provided the first opportunity in more than two decades to obtain spectral observations with a very large telescope. Seizing this chance, we conducted spectroscopic observations of 1998 KY_{26} using the 10.4-

Article published by EDP Sciences, to be cited as https://doi.org/10.1051/0004-6361/202659046

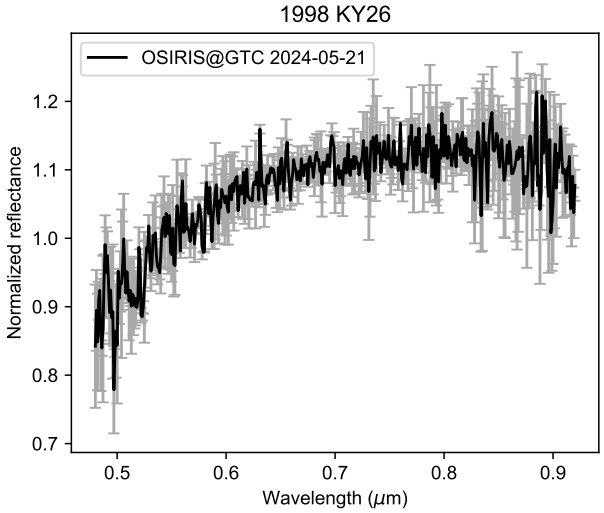

Fig. 1: Visible reflectance spectrum of 1998 KY_{26} observed with OSIRIS+ at the 10.4 m GTC on May 21, 2024. The averaged spectrum is shown in black, with the associated 1σ error of the average in gray.

meter Gran Telescopio Canarias (GTC). Located at the El Roque de los Muchachos Observatory on the island of La Palma in the Canary Islands, Spain, GTC is the one of the largest and most advanced optical and near-infrared telescope in the world. The spectroscopic data provide valuable insights into the asteroid's surface composition, potentially revealing its origin and evolutionary history.

The asteroid 1998 KY_{26} was observed on the night of May 21, 2024. Spectroscopic observations were done using the OSIRIS+ camera-spectrograph (Cepa et al. 2000; Cepa 2010), under the program GTC37-24A (PI, J. de León). OSIRIS+ is equipped with a blue-sensitive monolithic $4,096 \times 4,096$ pixels Charge-Coupled Device (CCD), which provides a $7.8' \times 7.8'$ field of view. We used the R300R grism that covers a wavelength range from 0.48 to 0.92 μm with a dispersion of 7.74 Å/pixel for a $0.6''$ slit. We combined the R300R grism with a $1.2''$ slit, oriented toward the parallactic angle, and with the telescope tracking rate set to match the asteroid's proper motion. Two consecutive spectra of 900 s each (starting time 04:14 UTC and 04:30 UTC, respectively), at an air mass of 1.36 were obtained. To obtain the asteroid's reflectance spectrum, we also observed the solar analog star Landolt SA112-1333 (three individual images of 1 s each), using the same instrumental setup and at a similar air mass to that of the asteroid. At the moment of the observations, 1998 KY_{26} presented an apparent visual magnitude of m_V=20.4, a phase angle of 29.7 degrees, and was at a distance of 1.053 au and 0.047 au from the Sun and Earth, respectively.

Data reduction was done using standard procedures. The 2D images were initially bias and flat-field corrected, the sky background was subtracted, and a 1D spectrum was extracted using a variable aperture, set to the pixel where the intensity was 10% of the peak value. Wavelength calibration was performed using Xe+Ne+HgAr lamps. This procedure was applied to the spectra of the asteroid and the solar analog star. To obtain the reflectance spectrum, we divided the asteroid observations by the spectra of the G2V star, and the resulting ratios were then averaged and normalized to unity at 0.55 μm to obtain the final reflectance spectrum of 1998 KY_{26}, shown in Fig. 1.

3. Spectral analysis

To estimate the composition of 1998 KY_{26}, we first carried out a taxonomic classification based on its spectral properties and albedo, then compared its spectral curve with those of meteorites available in the RELAB database (Pieters & Hiroi 2004). Both analyses are described in the subsections below.

3.1. Taxonomic classification

Accurate characterization of asteroid surface composition is required for understanding their formation and evolution. To this end, various asteroid taxonomic classifications have been proposed, each leveraging different spectral features and wavelength ranges. Among these, the Bus-DeMeo taxonomy (DeMeo et al. 2009) is one of the most widely adopted and comprehensive systems. This classification scheme utilizes reflectance spectra spanning a broad wavelength range from 0.45 to 2.45 μm, allowing for the identification of key absorption features related to mineralogical composition.

The Bus-DeMeo taxonomy broadly categorizes asteroids into groups based on the presence or absence of a characteristic absorption feature around 1 μm, which is typically indicative of olivine and pyroxene minerals. Further subdivisions are made based on spectral slope, other absorption bands, and the overall shape of the reflectance spectrum. To classify the reflectance spectrum of 1998 KY_{26}, we employed the M4AST online tool[1] (Popescu et al. 2012). This tool performs a χ^2 fitting curve-matching procedure (based on various criteria such as χ^2 or least-squares differences) , comparing the observed asteroid spectrum with a library of mean spectra for each taxonomic class defined by DeMeo et al. (2009). Using M4AST (see Fig. 2), our analysis yields a best fit to the Xe-type.

The Mahlke taxonomy (Mahlke et al. 2022), a more recent classification scheme, incorporates both reflectance spectra (0.45–2.45 μm) and albedo data. When evaluating our spectrum within this framework using the `classy` tool (Mahlke et al. 2022), we found that in the latent space, the S-type and E-type clusters are distributed in close proximity, making them difficult to distinguish when only limited visible wavelength information is available. Given the limited wavelength coverage of our data, which may not fully capture the diagnostic features required for a robust transformation into the latent space, we prioritized a direct comparison of spectral similarity via χ^2 minimization. Based on a χ^2 minimization analysis, we identified the M-type as the most probable classification, followed by the X-type. Both the Bus-DeMeo and Mahlke schemes consistently place the object within the X-complex. Notably, while the Xe-type in the Bus-DeMeo system closely aligns with the M- or X-types in the Mahlke taxonomy, the E-type exhibits a significantly redder spectral slope (Fig. 2).

This complex is further subdivided into E-, M-, and P-types, originally defined in the Tholen taxonomy (Tholen 1984). The geometric albedo p_V of E-type asteroids is $0.55^{+0.14}_{-0.11}$, while that of M-type asteroids is $0.14^{+0.05}_{-0.04}$, and that of P-type asteroids is $0.05^{+0.02}_{-0.01}$ (Mahlke et al. 2022). Xe-type asteroids in Bus & Binzel (2002a) are spectroscopically distinguished by a relatively broad and a subtle absorption band centered around 0.49 μm. This feature has been tentatively linked to the presence of troilite (FeS) and/or other opaque minerals, though its exact mineralogical interpretation can be complex. However, this feature of Xe-type asteroids is barely seen in the extended taxonomy

[1] `https://spectre.imcce.fr/m4ast/index.php/index/home`

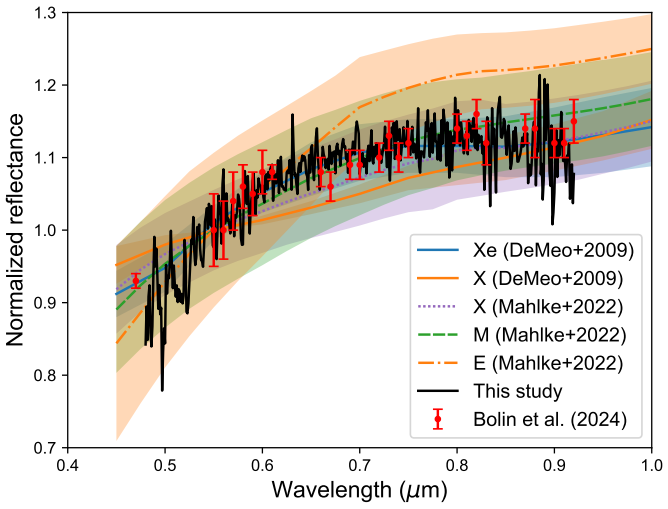

Fig. 2: Reflectance spectrum of 1998 KY_{26} (black) compared with the three best-matching taxonomic reference spectra from DeMeo et al. (2009) and Mahlke et al. (2022). The spectra obtained by Bolin et al. (2025) is also depicted in red.

using visible-to-near-infrared range by DeMeo et al. (2009). We observe a drop-off in reflectance in our spectrum of 1998 KY_{26} below ~0.56 μm, which could be attributed to the 0.49 μm band. However, the limited wavelength coverage of our observations and the relatively low signal-to-noise ratio of the spectrum in this wavelength range do not allow us to conclude that this band is present. Despite these challenges, our spectroscopic results are notably consistent with previous observations of 1998 KY_{26} obtained with the 8.1-meter Gemini North telescope, as reported by Bolin et al. (2025), further corroborating our taxonomic classification (see red points in Fig. 2). This consistency across independent observations strengthens the reliability of our Xe-class assignment.

Recent thermal infrared observations with VLT/VISIR further constrain the physical properties of 1998 KY_{26}. Beniyama et al. (2025) conducted deep mid-infrared imaging over three consecutive nights in May 2024. The asteroid was not detected, yielding a 10.64 μm flux density upper limit of $\sim$ 2 mJy. Thermophysical modeling based on this non-detection implied that the effective diameter of 1998 KY_{26} had to be smaller than 17 m, significantly below the radar-based estimate of 30±10 m (Ostro et al. 1999). This new size constraint, combined with an updated absolute magnitude of $H = 26.13 \pm 0.16$, requires a geometric albedo of $p_V \geq 0.19$. Such a high albedo is inconsistent with typical carbonaceous asteroids.

Recent independent constraints on the physical properties of 1998 KY_{26} strongly reinforce its classification as an E-type asteroid. Based on an extensive light curve campaign, (Santana-Ros et al. 2025) determined an absolute magnitude of $H = 26.13 \pm 0.16$. Combined with their size estimate of 11 ± 2 m, this implies a geometric albedo of $p_V \sim 0.52 \pm 0.08$. Such a high albedo is fully consistent with E-types.

Our GTC reflectance spectrum places 1998 KY_{26} in the Xe class of the Bus–DeMeo taxonomy, in the M or X class of the Malhke taxonomy, and in the X class of the Tholen taxonomy. This spectral classification, combined with the object's likely high albedo, points toward an interpretation as an E-type asteroid rather than M-type.

3.2. Comparison with meteorite spectra

To further constrain the composition of asteroid 1998 KY_{26}, we compared its reflectance spectrum with those of meteorites available in the RELAB database (Pieters & Hiroi 2004), using the M4AST tool, which computes the mean squared differences between normalized spectra of an asteroid and a meteorite. Note that due to the limited wavelength interval and the lack of absorption features in the observed spectrum, multiple spectral matches are possible. The best initial matches, which have the smallest mean squared spectral differences, correspond to two carbonaceous chondrites: a particulate (< 125 μm) sample of EET96029,14 (C2) and a sample of Murchinson (CM2) heated at 400°C. However, these materials are very dark, with reflectances on the order of 0.03 (3 %), and therefore inconsistent with the high albedo reported for this object.

Interestingly, the next best spectral match corresponds to a sample of an enstatite chondrite of type EL6, consistent with the previously reported taxonomic classification. This meteorite sample (#ID: MT-PFV-119-B) originates from the Allan Hills ALH 81021 meteorite, was processed in the laboratory, and consists of dry sieved, fine particulate material (<25 μm). Grossman (1994) noted that the enstatite in this sample is nearly pure $MgSiO_3$.

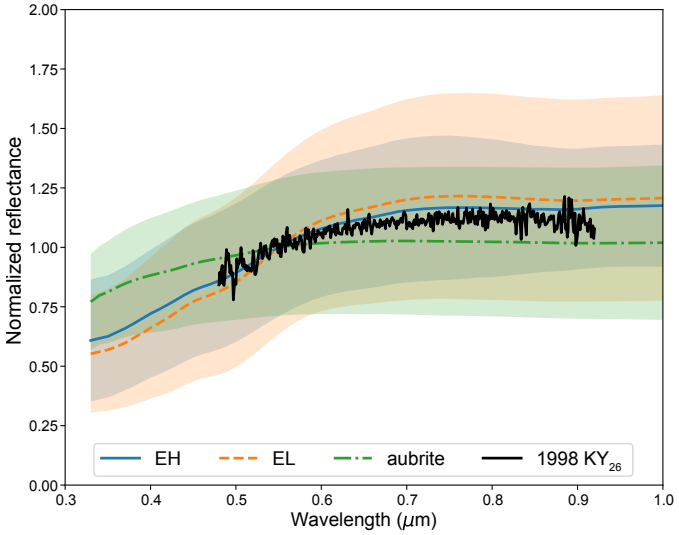

Fig. 3: Mean normalized reflectance spectra and standard deviation (shaded areas) for aubrites (dot-dashed green line), EH chondrites (solid blue line), and EL chondrites (dashed orange line) from the RELAB database, measured at a 30° phase angle. This highlights the flatter profile of aubrites versus the steeper slopes of enstatite chondrites. The spectrum of 1998 KY_{26} exhibits a shape consistent with EL/EH chondrites but a higher absolute reflectance typical of the aubrite group.

To further investigate this, we retrieved additional spectra from the RELAB database through the PDS Geoscience Node Spectral Library[2], including 40 aubrites (enstatite achondrites), 24 EH chondrites, and 29 EL chondrites, all measured at a 30° phase angle. Our analysis reveals significant disparity in reflectance at 0.55 μm (which can be grossly compared to the albedo) among these groups, despite their shared primary composition of enstatite. Aubrites exhibit a mean reflectance at 0.55 μm of 38 ± 11%, whereas EH and EL chondrites show significantly lower values of 10±3% and 11±4%, respectively. Further-

[2] https://pds-speclib.rsl.wustl.edu/

more, aubrites typically display a flatter spectral slope compared to the steeper profiles of EH and EL chondrites (Fig. 3). The spectrum of 1998 KY_{26} aligns closely with the spectral shape of EL and EH chondrites.

The average reflectance of the <25μm sample of the ALH 81021 EL6 chondrite (18% at a 30° phase angle) is higher than that for the EL chondrites group. By applying the conversion methodology defined in Eq. (2) of Beck et al. (2021), we derived an equivalent geometric albedo of 21%. This value is notably lower than the previous estimation reported by Santana-Ros et al. (2025); in terms of albedo alone, aubrites provide a closer analog to the asteroid's estimated properties.

4. Distribution of E-type asteroids

As described in the previous section, E-type asteroids are a subclass of X-types in Tholen's taxonomy. E-types are a relatively rare class characterized by their high albedo (typically $p_V > 0.3$) and distinctive spectral properties. Spectral similarity to enstatite achondrites (aubrites) was pointed out, for example, by Bell et al. (1989) and Gaffey et al. (1992). Historically, the Hungaria region, in the far inner asteroid belt with high inclination (~ 20 deg) has been recognized as the principal reservoir of these bodies (e.g., Gaffey et al. 1992; Clark et al. 2004). However, recent survey data have revealed that the distribution of E-types in the Solar System is more complex. Our investigation now focuses on the spectroscopic properties throughout the Hungaria region and the main belt, aiming to uncover further links to 1998 KY_{26}'s composition and history. This helps us understand its journey from its likely birthplace to its current near-Earth orbit.

For this analysis, we combined photometric data from the Sloan Digital Sky Survey (SDSS) small body catalog (Sergeyev & Carry 2021) with the albedo catalog (Mainzer et al. 2019) from the NEOWISE mission (Masiero et al. 2017). The SDSS provides five-band photometry in the u (354 nm), g (477 nm), r (623 nm), i (763 nm), and z (913 nm) filters. Following the data quality criteria described in Tatsumi et al. (2023, 2025), we selected only objects with reliable photometry (photometric errors < 0.1 mag in all bands, and no contamination flags). The photometric colors were converted into reflectance spectra using the following relation:

$$R_n = 10^{-0.4[(n-g)-(n-g)_\odot]}, \quad (1)$$

where n denotes the filter and $(n-g)_\odot$ represents the solar color as reported by Holmberg et al. (2006).

After reflectance spectra were normalized at the g band, we then identified X-class asteroid candidates based on their spectral slope between 0.2–0.6 μm^{-1} from g to z (based on DeMeo & Carry (2013)). To ensure reliability and exclude nonlinear spectra, we only selected candidates that exhibited a high correlation coefficient ($R^2 > 0.6$) in the linear fit to their reflectance. After classifying these candidates as X-types, we cross-matched them with the NEOWISE albedo catalog to obtain their geometric albedos (p_V). Finally, we defined E-type candidates as X-class asteroids with $p_V > 0.3$ based on Tholen's taxonomy. Using this procedure, we identified 252 possible E-type asteroids, including 54 of extremely high albedo $p_V > 0.5$ (Fig. 4). E-type asteroids, including those identified in the literature (see Appendix A for details), are widespread in the main belt. E-type asteroids with relatively low albedo ($0.3 < p_V < 0.5$) are clustered in some regions, possibly related to dynamical families: Eunomia, Maria, and Koronis. Note that the most extremely high albedo E-types concentrate in the Hungaria region and the low-inclination inner main belt (IMB) region.

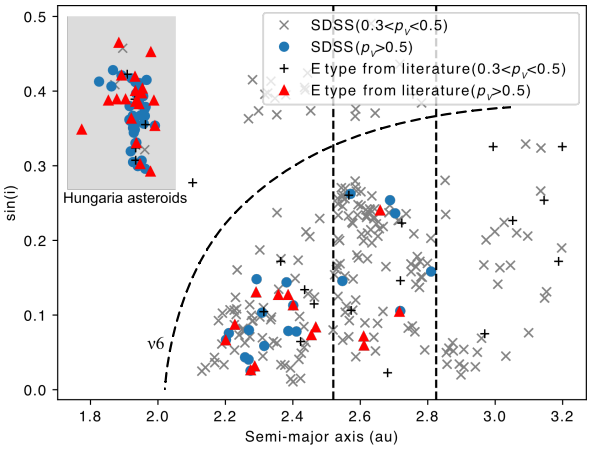

Fig. 4: Distribution of E-type candidates in the $a - \sin(i)$ plane. The gray crosses denote the SDSS E-type candidates with $0.3 \leq p_V \leq 0.5$. The blue circles denote the same candidates as the crosses but with $p_V > 0.5$. The black pluses represent the E-types reported in the literature with $0.3 \leq p_V \leq 0.5$. The red triangles represent the same candidates as the black pluses but with $p_V > 0.5$ (Appendix A). The gray hatched area indicates the Hungaria region, and the dashed lines represent the $\nu 6$ secular and the mean motion resonances.

5. Discussion

5.1. Dynamical pathway for 1998 KY_{26}

The dynamical origin of 1998 KY_{26} can be constrained using the near-earth object (NEO) population model (Granvik et al. 2018; Morbidelli et al. 2020; Nesvorný et al. 2023) described by Bolin et al. (2025). Their analysis indicates that the majority of near-Earth asteroids (NEAs) on KY_{26}-like orbits are supplied from the IMB, in particular through the ν_6 secular resonance, with a probability of about 67%. Additional contributions arise from the Hungaria region (~ 17%) and the 3:1 mean-motion resonance with Jupiter (~ 16%) Bolin et al. (2025); a more detailed consideration of the orbital inclination strongly favors an inner-belt origin.

Following the methodology of Bottke et al. (2015) for (101955) Bennu, we consider the efficiency of Yarkovsky-driven transport. For a small (diameter ~ 30 m) object such as 1998 KY_{26}, the Yarkovsky effect induces rapid semimajor axis drift, allowing it to reach the ν_6 resonance from the Nysa-Polana complex within a few million years. Notably, the low inclination of 1998 KY_{26} ($i \sim 1.49°$) is highly consistent with the low-inclination population of the IMB ($i < 5°$). In contrast, transporting an object from the high-inclination Hungaria region ($i \approx 18°$–$28°$) to a 1998 KY_{26}-like orbit would require an improbable degree of inclination evolution, as the ν_6 resonance and subsequent planetary encounters generally preserve or increase inclination unless specific close-approach geometries occur (Morbidelli et al. 2002; Bottke et al. 2015).

This strongly suggests that 1998 KY_{26} is more likely to originate from the IMB rather than the Hungarias, even though both reservoirs are known sources of high-albedo E-type asteroids.

The ν_6 resonance provides an efficient transport pathway from the vicinity of the Nysa family into Earth-crossing orbits on relatively short timescales ($\leq 10^7$ yr) (Scholl & Froeschle 1991). Such timescales are compatible with both the collisional lifetimes of small fragments in the main belt and the dynamical lifetime of NEAs (Morbidelli et al. 2002).

5.2. Spectral diversity and the bimodality of E-type asteroids

The diversity within the E-type population has been well established by previous spectroscopic studies. Based on visible and near-infrared observations, Clark et al. (2004) proposed three subgroups: E(I), characterized by featureless spectra consistent with nearly pure enstatite and represented by objects such as (64) Angelina and (434) Hungaria; E(II), showing a 0.49 μm absorption attributed to oldhamite (CaS), as seen in (2867) Steins and (3103) Eger; and E(III), exhibiting a 0.9 μm band due to Fe-bearing enstatite, with examples including (44) Nysa and (1251) Hedera. Gaffey & Kelley (2004) emphasized that these subgroups reflect different reducing formation environments, while Fornasier et al. (2008) argued that E-type spectra form a continuous sequence rather than three sharply separated classes.

To explore the diversity within E-type asteroids, we analyzed the objects identified as E-types in the SDSS sample. Figure 5 shows their distribution in the a^* versus $u-g$ plane, where

$$a^* = 0.89\,(g-r)_{\rm obj} + 0.45\,(r-i)_{\rm obj} - 0.57, \quad (2)$$

following Ivezić et al. (2001). Larger a^* values indicate a stronger $\sim$ 0.9 μm absorption band (i.e., more E(III)-like spectra), because the increased depression toward the i–z region reddens $r-i$ and thus raises a^*. The horizontal axis $u-g$ primarily traces the near-UV drop. The distribution is distinctly bimodal: one cluster, the "Convex" group, exhibits a convex continuum with the 0.9 μm absorption, consistent with the E(III) subtype, whereas the other, the "Linear" group, displays an approximately linear, featureless slope characteristic of E(I) (Fig. 6). We note that the narrow $\sim$ 0.49 μm absorption diagnostic of E(II) is not reliably constrained by SDSS broadbands, and thus E(II) cannot be robustly separated in this dataset.

We derived the SDSS band reflectances R_b ($b \in \{g, r, i\}$) from the GTC reflectance spectrum $R(\lambda)$ using a synthetic photometry approach. Instead of a local linear approximation, we computed the integrated reflectance for each band by convolving the spectrum with the SDSS filter transmission functions $T_b(\lambda)$ [3]:

$$R_b = \frac{\int R(\lambda) T_b(\lambda) d\lambda}{\int T_b(\lambda) d\lambda}. \quad (3)$$

To account for the limited wavelength coverage at the blue end of the g band, the spectrum was extrapolated using a second-order polynomial fit to the observed data.

Object colors follow from band-reflectance ratios,

$$(g-r)_{\rm KY_{26}} = (g-r)_\odot - 2.5\log_{10}\frac{R_g}{R_r}, \quad (4)$$

$$(r-i)_{\rm KY_{26}} = (r-i)_\odot - 2.5\log_{10}\frac{R_r}{R_i}, \quad (5)$$

where we correct for the contribution of the solar colors (Holmberg et al. 2006). Uncertainties on a^* were obtained by a Monte Carlo-like analysis: we drew $(R_g, R_r, R_i) \sim \mathcal{N}(R_b, \sigma_b)$ (independent) and recomputed a^* for 10,000 realizations; the reported value is the sample mean and its 1σ scatter. Finally, we calculated $a^* = 0.10 \pm 0.03$, shown as a gray hatch in Fig. 5. We could not calculate $u-g$ because the GTC spectrum lacks coverage at the wavelength in the u filter. The range of a^* suggests 1998 KY_{26} might belong to the "Convex" group.

[3] https://www.sdss4.org/instruments/camera/

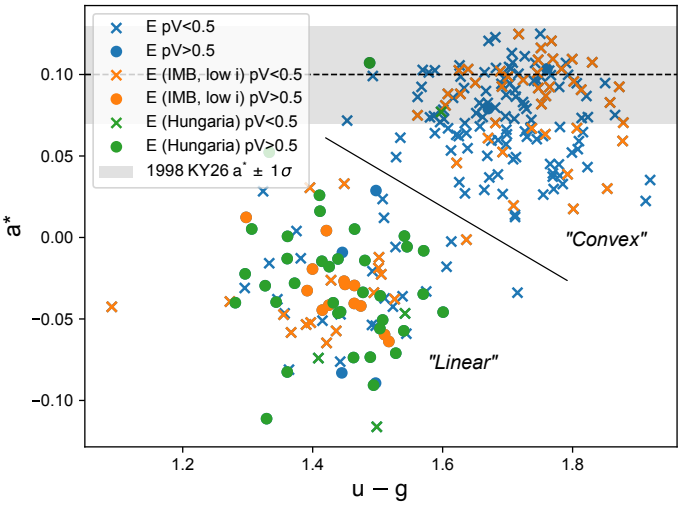

Fig. 5: Distribution of candidate E-type asteroids in the a^*–$(u-g)$ plane. The blue symbols represent the main E-type population (E); the orange symbols show the IMB low-inclination group (E (IMB, low i)); and the green symbols correspond to the Hungaria group (E (Hungaria)). The marker shapes indicate geometric albedo: crosses for $p_V < 0.5$ and circles for $p_V \geq 0.5$. A horizontal shaded band indicates the $a^* \pm 1\sigma$ range for 1998 KY_{26}, with the mean a^* shown as a dashed line. The two clusters, "Linear" (lower a^*) and "Convex" (higher a^*), are separated in this space.

Figure 5 further separates the SDSS E-type sample into dynamical subpopulations. We classified the sample using dynamical cuts: the Hungaria population defined by $1.8 \leq a \leq 2.0$ au and $0.25 \leq \sin i \leq 0.5$, and the low-inclination IMB group defined by $2.0 \leq a \leq 2.52$ au and $0 \leq \sin i \leq 0.2$. Most of the Hungaria population (green) has high geometric albedo ($p_V > 0.5$) and falls in the "Linear" cluster, consistent with the classification of (434) Hungaria as E(I). By contrast, the IMB, low-inclination E types (likely related to the Nysa complex; orange) populate both clusters: their $p_V > 0.5$ subset overlaps the Hungaria members in the "Linear" cluster; nevertheless, several IMB objects with only moderate albedo still belong to the "Linear" group as well.

Given this context, 1998 KY_{26} shows a convex continuum across the visible and hints at a $\sim$ 0.9 μm absorption, placing it in our "Convex" cluster and making it more akin to E(III) exemplars such as (44) Nysa than to the "Linear," E(I)-like Hungarias. Although the $\sim$ 0.9 μm feature is not unambiguously detected in KY_{26} due to observational limitations, the overall curvature argues for a closer affinity with the Nysa-like E(III) population than with the Hungaria E(I) group, supporting an IMB origin.

5.3. Nysa family and its parent body

The Nysa region of the IMB ($a \simeq 2.41-2.50$ au, $e \simeq 0.12-0.21$, $i \simeq 1-10°$) represents one of the most compositionally complex zones in the asteroid belt, characterized by the coexistence of diverse taxonomic groups including C, S, and X (E/M). What

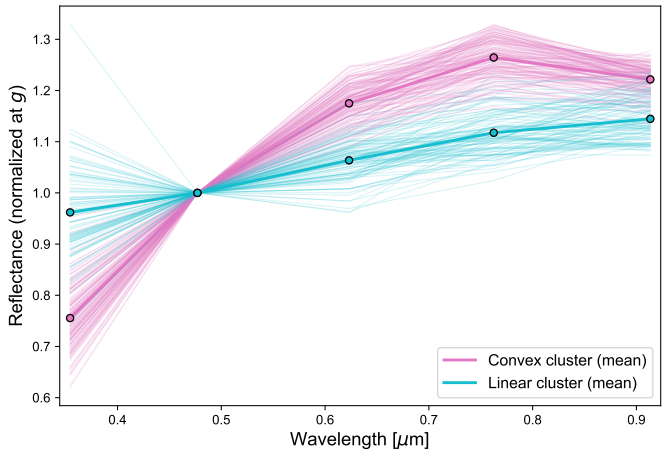

Fig. 6: Reflectance spectra for the SDSS E-type sample by cluster. Each thin curve shows an individual object's reflectance spectra normalized at the g band (0.48 μm). The thick colored curves represent the cluster means ("Linear" and "Convex"). The clusters are defined in the a^*–$(u-g)$ plane (Fig. 5).

has historically been referred to as the "Nysa-Polana family" is now understood to be a superposition of several overlapping clusters with distinct spectral properties. Earlier work emphasized this complexity: Cellino et al. (2001) argued that the Nysa–Polana clan is a superposition of distinct families and that high-albedo asteroids possibly associated with (44) Nysa coexist with the low-albedo C-type population of the Polana–Eulalia families. Walsh et al. (2013) identified Eulalia and redefined Polana as two separate low-albedo families, while in later work by de León et al. (2016) in the visible and Pinilla-Alonso et al. (2016) in the near-infrared showed that these two families had identical spectra. Moreover, an additional group of M- and S-type objects, possibly related to (135) Hertha, were found (e.g., Cellino et al. 2001; Fornasier et al. 2008). Dykhuis & Greenberg (2015) further subdivided the region into Hertha 1 (S-type), Hertha 2 (X-type), Polana, and two Eulalia families, concluding that (44) Nysa is likely an isolated E-type interloper.

Note that both (44) Nysa and (135) Hertha exhibit spectral shapes that can be broadly associated with the X-complex. However, their physical properties diverge significantly. Nysa is a high-albedo object ($p_V \sim 0.48$) and is spectrally classified as an E(III)-type, exhibiting the 0.9 μm absorption band characteristic of Fe-bearing enstatite. In contrast, Hertha has a much lower albedo ($p_V \sim 0.14$) despite its X-type-like spectral continuum, placing it closer to the M- or even low-end S-type regime. The coexistence of E- and M-type objects within the same dynamical region further underscores the compositional complexity of the Nysa–Polana–Hertha complex.

To investigate the albedo distribution of the Nysa–Polana complex, we cross–matched the Nysa–Polana family membership list by Nesvorný et al. (2015) with the NEOWISE catalog (Mainzer et al. 2019) and extracted the geometric albedo p_V. The resulting distribution exhibits a prominent bimodal structure, though the high-albedo group shows a broad and asymmetric spread. This comprises a group of low–albedo asteroids (Polana-like) and a distinct group of high–albedo asteroids (Nysa and Hertha-like). To quantitatively characterize this complex structure and account for the observed asymmetry, we fitted the geometric albedo histogram using a Gaussian mixture model (GMM) with three components (Fig. 7). The model was optimized with the expectation–maximization algorithm, assuming full covariance matrices.

The fitted model converged to three distinct Gaussian components with mean albedos of approximately 0.06, 0.23, and 0.35, possibly corresponding to the dark Polana–Eulalia complex, an intermediate Hertha cluster, and the bright Nysa group, respectively. This analysis shows significant high-albedo members in this dynamical region, suggesting the coexistence of at least four independent families: Nysa, Hertha, Polana, and Eulalia.

Our identification of a statistically significant cluster of high-albedo objects indicates that Nysa is not simply an isolated body but the largest member of a distinct Nysa family. This finding highlights an overlooked E-type reservoir in the IMB, which could serve as an additional source of high-albedo near-Earth asteroids such as 1998 KY_{26}.

This albedo distribution provides a key link to meteorite analogs. The intermediate albedo component ($p_V \sim 0.23$) is consistent with enstatite chondrites. For instance, the <25μm sample of EL6 chondrite ALH 81021 has a reflectance of 18%, converted to an equivalent geometric albedo of 21%. While this matches the Hertha-like component, it is significantly lower than the $p_V \sim 0.52$ estimated for 1998 KY_{26} (Santana-Ros et al. 2025). In contrast, aubrites (enstatite achondrites) typically exhibit equivalent geometric albedos exceeding 0.4. As shown by Clark et al. (2004), the high albedo of E(III) objects is best reproduced by differentiated aubritic material. The high albedo of 1998 KY_{26} therefore strongly suggests it is a fragment of a differentiated E-type crust, akin to (44) Nysa, rather than an undifferentiated enstatite chondritic body.

Moreover, the reflectance spectrum of 1998 KY_{26} provides an intriguing link between Nysa and Hertha. While its high geometric albedo ($p_V \sim 0.52$) is fully consistent with an E-type classification and hence with Nysa ($p_V \sim 0.48$), its spectral shape more closely resembles that of Hertha, showing a similar convex continuum in the visible range (see Fig. 8). The coexistence of Nysa-like albedo and Hertha-like spectral morphology in 1998 KY_{26} suggests that these two large bodies may share a deeper genetic connection. One possible interpretation is that Nysa and Hertha could be remnants of a common differentiated parent body (Tedesco et al. 1982), with 1998 KY_{26} representing a small fragment sampling both the high-albedo enstatite-rich component (as seen in Nysa) and the spectral slope characteristics typical of Hertha.

In this view, 1998 KY_{26}, representing a "hybrid" fragment—a polymict rock sampled from the boundary between the high-albedo crust and the deeper, more iron-rich layers—serves as direct evidence linking these two populations resulting from the large-scale disruption of their common progenitor. Importantly, the forthcoming Hayabusa2 rendezvous with 1998 KY_{26} will provide the first opportunity to directly examine such a fragment in situ. By characterizing its surface composition and physical properties at close range, the mission may resolve the long-standing puzzle of whether E-type Nysa and M-type Hertha share a common parent body and thereby shed new light on the collisional and differentiation history of the IMB.

6. Conclusions

We presented new GTC spectroscopic observations and a reanalysis of albedo distributions in the Nysa–Polana complex to investigate the nature and origin of the Hayabusa2# target, 1998 KY_{26}. The GTC spectrum indicates an X-type in Tholen's taxonomy and Xe-type in Bus-DeMeo's taxonomy. When combined

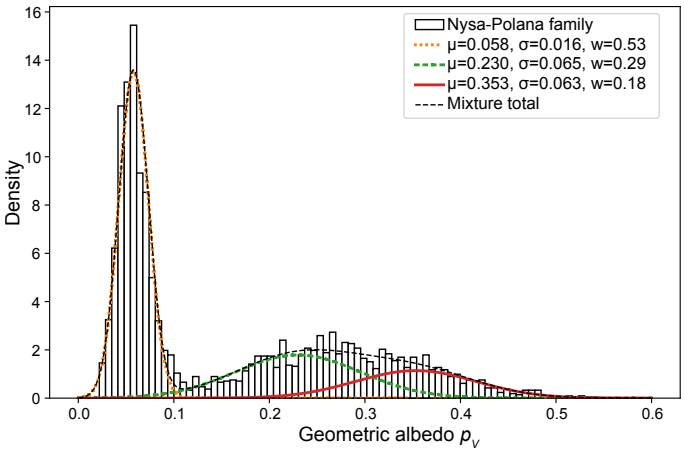

Fig. 7: Distribution of the geometric albedo (p_V) for members of the Nysa-Polana complex, cross-matched with NEOWISE. The histogram is fitted with a three-component GMM. The color curves represent the individual fitted components, defined by their mean albedo (μ), standard deviation (σ), and mixing weight (w), corresponding to the dark Polana-Eulalia complex ($p_V \sim 0.06$), an intermediate Hertha group ($p_V \sim 0.23$), and the bright Nysa group ($p_V \sim 0.35$).

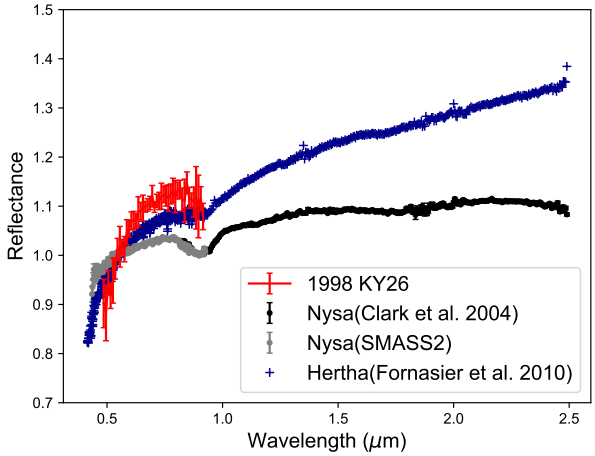

Fig. 8: GTC visible reflectance spectrum of 1998 KY_{26} (red) compared with the visible spectra of (44) Nysa from (Bus & Binzel 2002b) (gray), its near-infrared spectrum from (Clark et al. 2004) (black), joined using their common wavelength interval of 0.8–0.9 μm, and the spectrum of (135) Hertha from Fornasier et al. (2010) (blue).

with independent albedo constraints ($p_V \sim 0.52$), 1998 KY_{26} is best interpreted as an E-type asteroid.

In the a^*–$(u-g)$ plane, SDSS E-types separate into a featureless "Linear" cluster (E[I]) and a "Convex" cluster with stronger $\sim$ 0.9 μm absorption (E[III]); the narrow $\sim$ 0.49 μm E(II) band cannot be isolated with SDSS broadbands. Most of the Hungaria population has $p_V > 0.5$ and lies in the "Linear" cluster, while the low-inclination IMB E-types (Nysa-related) populate both clusters, including "Linear" members with only moderate albedo. For 1998 KY_{26}, we estimate $a^* = 0.11 \pm 0.08$. Its convex continuum and permitted a^* range favor the "Convex"/E(III) group and an IMB (Nysa) origin over Hungaria.

Our GMM analysis of NEOWISE albedos confirms that the Nysa-Polana region hosts multiple overlapping families, including low-albedo Polana and Eulalia groups, an intermediate-albedo Hertha cluster, and a distinct high-albedo population associated with (44) Nysa. While previous work from Dykhuis & Greenberg (2015) considered Nysa to be an isolated E-type object, our results identify a statistically significant cluster of high-albedo asteroids in this region, supporting the existence of a previously unrecognized Nysa family.

The spectrum of 1998 KY_{26} resembles that of Hertha in its overall convex continuum while maintaining the high albedo typical of Nysa, suggesting a possible genetic link between the two large bodies. This hybrid nature supports the classical model of Tedesco et al. (1982), wherein Nysa and Hertha represent different layers of a single differentiated parent body. In particular, 1998 KY_{26} displays a convex spectral morphology closer to the E(III)-type Nysa than to the nearly linear E(II)-type Hungarias, and dynamical models indicate that KY26-like orbits are most likely supplied through ν_6 resonance (Bolin et al. 2025). Taken together, these results strongly suggest that 1998 KY_{26} originated from the Nysa family rather than the Hungaria region.

The upcoming Hayabusa2 rendezvous with 1998 KY_{26} in 2031 offers a unique opportunity to test these hypotheses. In situ measurements of this small, optically bright, rapidly rotating asteroid will directly constrain its composition and surface properties, potentially resolving whether Nysa and Hertha share a common parent body and shedding new light on the collisional and differentiation history of the IMB.

Acknowledgements. We would like to express our sincere gratitude to the anonymous referee for the insightful comments. This work is supported by JAXA Hayabusa2# International Visibility Enhancement Project. ET acknowledges support from Spanish government - Ayuda Ramón y Cajal 2023 (RYC2023-043483-I). JdL acknowledges support from the Agencia Estatal de Investigacion del Ministerio de Ciencia e Innovación (AEI-MCINN) under grant "Hydrated Minerals and Organic Compounds in Primitive Asteroids" with reference PID2020-120464GB-100. Based on observations made with the Gran Telescopio Canarias (GTC), installed at the Spanish Observatorio del Roque de los Muchachos of the Instituto de Astrofísica de Canarias, on the island of La Palma. This research utilizes spectra with the NASA RELAB facility at Brown University.

References

Barucci, M. A., Fulchignoni, M., Fornasier, S., et al. 2005, A&A, 430, 313
Beck, P., Schmitt, B., Potin, S., Pommerol, A., & Brissaud, O. 2021, Icarus, 354, 114066
Bell, J. F., Davis, D. R., Hartmann, W. K., & Gaffey, M. J. 1989, in Asteroids II, ed. R. P. Binzel, T. Gehrels, & M. S. Matthews, 921–945
Beniyama, J., Müller, T. G., Delbo, M., et al. 2025, Astronomical Journal, 169, 264
Beniyama, J., Sako, S., Ohtsuka, K., et al. 2023, ApJ, 955, 143
Bolin, B. T., Fremling, C., Belyakov, M., et al. 2025, AJ, 169, 303
Bottke, W. F., Vokrouhlický, D., Walsh, K. J., et al. 2015, Icarus, 247, 191
Brown, P. G., Assink, J. D., Astiz, L., et al. 2013, Nature, 503, 238
Bus, S. J. & Binzel, R. P. 2002a, Icarus, 158, 146
Bus, S. J. & Binzel, R. P. 2002b, Icarus, 158, 106
Cellino, A., Zappalà, V., Doressoundiram, A., et al. 2001, Icarus, 152, 225
Cepa, J. 2010, in Astrophysics and Space Science Proceedings, Vol. 14, Highlights of Spanish Astrophysics V, 15
Cepa, J., Aguiar, M., Escalera, V. G., et al. 2000, in Society of Photo-Optical Instrumentation Engineers (SPIE) Conference Series, Vol. 4008, Optical and IR Telescope Instrumentation and Detectors, ed. M. Iye & A. F. Moorwood, 623–631
Clark, B. E., Bus, S. J., Rivkin, A. S., Shepard, M. K., & Shah, S. 2004, Journal of Geophysical Research: Planets, 109, E02001
de León, J., Pinilla-Alonso, N., Delbo, M., et al. 2016, Icarus, 266, 57
DeMeo, F. & Binzel, R. P. 2008, Icarus, 194, 436
DeMeo, F. & Carry, B. 2013, Icarus, 226, 723
DeMeo, F. E., Binzel, R. P., Slivan, S. M., & Bus, S. J. 2009, Icarus, 202, 160
Dykhuis, M. J. & Greenberg, R. 2015, Icarus, 252, 199
Fornasier, S., Clark, B. E., Dotto, E., et al. 2010, Icarus, 210, 655

Fornasier, S., Migliorini, A., Dotto, E., & Barucci, M. A. 2008, Icarus, 196, 119
Gaffey, M. J. & Kelley, M. S. 2004, in Lunar and Planetary Science Conference, Lunar and Planetary Science Conference, 1812
Gaffey, M. J., Reed, K. L., & Kelley, M. S. 1992, Icarus, 100, 95
Granvik, M., Morbidelli, A., Jedicke, R., et al. 2018, Icarus, 312, 181
Grossman, J. N. 1994, Meteoritics, 29, 100
Harris, A. W., Mueller, M., Delbó, M., & Bus, S. J. 2007, Icarus, 188, 414
Hirabayashi, M., Mimasu, Y., Sakatani, N., et al. 2021, Advances in Space Research, 68, 1533
Holmberg, J., Flynn, C., & Portinari, L. 2006, MNRAS, 367, 449
Ivezić, Ž., Tabachnik, S., Rafikov, R., et al. 2001, The Astronomical Journal, 122, 2749
Kikuchi, S., Mimasu, Y., Takei, Y., et al. 2023, Acta Astronautica, 211, 295
Lazzaro, D., Angeli, C. A., Carvano, J. M., et al. 2004, Icarus, 172, 179
Mahlke, M., Carry, B., & Mattei, P.-A. 2022, A&A, 665, A26
Mainzer, A., Bauer, J., Cutri, R.and Grav, T., et al. 2019, NASA Planetary Data System
Masiero, J. R., Nugent, C., Mainzer, A. K., et al. 2017, AJ, 154, 168
Morbidelli, A., Bottke, W., Froeschlé, C., Michel, P., et al. 2002, Asteroids iii, 409
Morbidelli, A., Delbo, M., Granvik, M., et al. 2020, Icarus, 340, 113631
Nesvorný, D., Brož, M., & Carruba, V. 2015, in Asteroids IV, 297–321
Nesvorný, D., Deienno, R., Bottke, W. F., et al. 2023, AJ, 166, 55
Ostro, S. J., Pravec, P., Benner, L. A. M., et al. 1999, Science, 285, 557
Pieters, C. M. & Hiroi, T. 2004, in Lunar and Planetary Science Conference, Lunar and Planetary Science Conference, 1720
Pinilla-Alonso, N., de León, J., Walsh, K., et al. 2016, Icarus, 274, 231
Popescu, M., Birlan, M., & Nedelcu, D. A. 2012, A&A, 544, A130
Popescu, M. M., Văduvescu, O., de León, J., et al. 2023, A&A, 676, A126
Reddy, V., Kelley, M. S., Benner, L., et al. 2024, The Planetary Science Journal, 5, 141
Rivkin, A. S., Mueller, T., MacLennan, E., et al. 2025, Research Notes of the American Astronomical Society, 9, 70
Santana-Ros, T., Bartczak, P., Muinonen, K., et al. 2025, Nature Communications, 16, 8275
Scholl, H. & Froeschle, C. 1991, A&A, 245, 316
Sergeyev, A. V. & Carry, B. 2021, A&A, 652, A59
Tatsumi, E., Vilas, F., de León, J., et al. 2025, A&A, 693, A140
Tatsumi, E., Vilas, F., de León, J., et al. 2023, A&A, 672, A189
Tedesco, E. F., Tholen, D. J., & Zellner, B. 1982, AJ, 87, 1585
Tholen, D. J. 1984, PhD thesis, University of Arizona, Tucson
Walsh, K. J., Delbó, M., Bottke, W. F., Vokrouhlickỳ, D., & Lauretta, D. S. 2013, Icarus, 225, 283
Xu, S., Binzel, R. P., Burbine, T. H., & Bus, S. J. 1995, Icarus, 115, 1

Appendix A: E type asteroids from the literature

We cataloged E-type asteroids identified in earlier work in Table A.1. X/Xe-class objects were considered E type if their geometric albedo was greater than 0.3 ($p_V > 0.3$).

Table A.1: E-type asteroids from the literature.

Number	Name	Subtype	p_V	a	e	i	H	Tax.	Ref.	Fam.
44	Nysa	E(III)	0.482	2.423	0.149	3.7	7.03	E, Xc	T86, BB02, C04	Nysa-Polana
64	Angelina	E(II)	0.483	2.681	0.126	1.3	7.67	E, Xe	T86,BB02, D09, C04	
71	Niobe		0.369	2.756	0.173	23.3	7.30	Xe	BB02	Gallia
92	Undina		0.341	3.188	0.104	9.9	6.61	Xc	BB02, D09	
214	Aschera	E(III)	1.000	2.611	0.032	3.4	9.20	E	T86, C04	
317	Roxane	E(III)	0.926	2.287	0.086	1.8	10.03	E, Xe	T86, BB02, C04	
399	Persephone		0.311	3.052	0.073	13.1	9.00	X	BB02	
422	Berolina		0.716	2.228	0.215	5.0	10.83	X	L04	
434	Hungaria	E(I or II)	0.726	1.944	0.074	22.5	11.21	E, Xe, X	T86, BB02, L04, D09	Hungaria
437	Rhodia	E(III)	0.677	2.386	0.249	7.3	10.41	X	L04	
504	Cora	E(I)	0.341	2.723	0.216	12.9	10.13	X	BB02,F08	
523	Ada		0.351	2.969	0.174	4.3	9.90	X	BB02	
620	Drakonia	E(III)	0.419	2.435	0.135	7.7	11.28	E	T86	
665	Sabine		0.494	3.145	0.171	14.7	8.70	X	L04	
678	Fredegundis		0.344	2.573	0.218	6.1	9.02	X	BB02	
727	Nipponia		0.479	2.566	0.106	15.1	9.60	X	L04	Maria
741	Botolphia		0.337	2.719	0.071	8.4	10.00	X	BB02	
815	Coppelia		0.644	2.659	0.076	13.9	10.70	Xe, X	BB02, L04	
1025	Reima		1.000	1.979	0.039	26.9	12.50	E, Xe, X	T86, BB02, L04	
1063	Aquilegia		0.389	2.314	0.040	6.0	11.38	X	X99	
1103	Sequoia	E(III)	0.384	1.934	0.095	17.9	12.25	E, X	T86,BB02, C04	Hungaria
1155	Aenna		0.356	2.463	0.164	6.6	12.00	Xe	BB02	
1251	Hedera	E(III)	0.636	2.716	0.158	6.0	10.50	E, X	T96,BB02, C04	
1304	Arosa		0.337	3.199	0.117	19.0	9.20	X	BB02	
1355	Magoeba		0.582	1.853	0.045	22.8	13.05	X	L04	
1653	Yakhontovia		0.599	2.610	0.323	4.1	11.60	X	BB02	
1919	Clemence		0.686	1.936	0.095	19.3	13.45	X	L04	Hungaria
2001	Einstein		0.810	1.934	0.099	22.7	12.85	Xe, X	BB02, L04	
2035	Stearns		0.649	1.884	0.132	27.7	12.61	E, Xe	T86, BB02, D09	
2048	Dwornik	E(I or II)	1.000	1.954	0.043	23.8	13.50	E	T86, C04	
2086	Newell		0.571	2.401	0.112	6.5	12.30	Xc	BB02	Vesta
2303	Retsina		0.341	2.994	0.117	19.0	11.20	X	L04	
2449	Kenos	E(I)	0.387	1.909	0.168	25.0	14.26	E	T86	
2491	Tvashtri		0.561	1.878	0.054	22.9	13.68	X	L04	
2577	Litva		0.593	1.904	0.138	22.9	13.18	EU, A	T86, F08	
2736	Ops		0.848	2.291	0.085	7.5	13.10	Xc	BB02	
2867	Steins	E(II)	0.300	2.364	0.146	9.9	13.14	E	B05	
3101	Goldberger			1.979	0.047	28.6	14.13	X	L04	
3103	Eger	E(II)	0.640	1.404	0.354	20.9	15.38	Xe	BB02, D09	
3169	Ostro		0.960	1.892	0.067	24.9	12.73	Xe	BB02	Hungaria
3381	Mikkola		0.639	2.455	0.205	4.2	13.20	X	X99	
3447	Burckhalter		0.779	1.991	0.029	20.7	12.30	X	L04	
3483	Svetlov		0.827	1.933	0.125	23.6	13.70	X	L04	Hungaria
3691	Bede		0.515	1.774	0.284	20.4	14.70	Xc	BB02	
3762	Amaravella		0.507	2.275	0.078	1.5	13.50	X	BB02	
3880	Kaiserman		0.566	1.947	0.083	17.6	13.70	X	L04	Hungaria
3940	Larion		0.566	1.988	0.056	22.8	12.70	X	L04	
3958	Komendantov		0.610	2.468	0.208	4.8	12.30	Xc	BB02	
4031	Mueller		0.389	1.934	0.101	18.9	13.10	X	X99	Hungaria
4205	David Hughes			1.727	0.149	16.5	14.30	Xe	BB02	
4440	Tchantches		1.000	1.921	0.077	21.3	13.60	X	X99	
4660	Nereus		0.550	1.485	0.359	1.5	18.75	Xe	BB02	
4764	Joneberhart		0.803	1.932	0.047	24.8	14.00	X	L04	Hungaria
4786	Tatianina		0.514	2.357	0.194	7.3	13.30	Xc	BB02	
4942	Munroe		0.936	2.201	0.136	3.8	13.50	X	BB02	
5751	Zao		0.360	2.103	0.424	16.1	14.80	X	BB02, L04	

Table A.1: continued.

Number	Name	Subtype	p_V	a	e	i	H	Tax.	Ref.	Fam.
6394	1990 QM2		0.615	1.939	0.093	22.8	13.70	X	L04	Hungaria
6435	Daveross	E(I)		1.919	0.058	23.4	15.36	E	F08	Hungaria
6461	Adam		0.543	1.952	0.102	23.4	14.20	X	L04	Hungaria
6911	Nancygreen	E(II)	0.392	1.932	0.090	22.9	14.30	E	F08	
7579	1990 TN1		0.518	1.978	0.065	17.0	13.81	E, A	F08	Hungaria
33342	1998 WT24		0.654	0.719	0.418	7.4	18.02	E	H07	
745311	2010 XC15		0.350	0.732	0.420	8.2	21.48	E	B23	

References. T86 = Tholen (1984); BB02 = Bus & Binzel (2002a); C04 = Clark et al. (2004); L04 = Lazzaro et al. (2004); D09 = DeMeo & Binzel (2008); F08 = Fornasier et al. (2008); B05 = Barucci et al. (2005); X99 = Xu et al. (1995); H07 = Harris et al. (2007); B23 = Beniyama et al. (2023)